Rapid Communications

Electrical and thermal transport in antiferromagnet-superconductor junctions

Martin F. Jakobsen,[1] Kristian B. Naess,[1] Paramita Dutta,[2,3] Arne Brataas,[1] and Alireza Qaiumzadeh[1]

[1] *Center for Quantum Spintronics, Department of Physics, Norwegian University of Science and Technology, NO-7491 Trondheim, Norway*

[2] *Department of Physics and Astronomy, Uppsala University, Box 516, S-751 20 Uppsala, Sweden*

[3] *Institute of Physics, Sachivalaya Marg, Bhubaneswar 751005, India*

(Received 5 June 2020; revised 5 October 2020; accepted 7 October 2020; published 23 October 2020)

We demonstrate that antiferromagnet-superconductor (AF-S) junctions show qualitatively different transport properties than normal metal–superconductor (N-S) and ferromagnet-superconductor (F-S) junctions. We attribute these transport features to the presence of two different scattering processes in AF-S junctions, i.e., specular reflection of holes and retroreflection of electrons. Using the Blonder-Tinkham-Klapwijk formalism, we find that the electrical and thermal conductances depend nontrivially on antiferromagnetic exchange strength, voltage, and temperature bias. Furthermore, we show that the interplay between the Néel vector direction and the interfacial Rashba spin-orbit coupling leads to a large anisotropic magnetoresistance. The unusual transport properties make AF-S interfaces unique among the traditional condensed-matter-system-based superconducting junctions.

DOI: 10.1103/PhysRevB.102.140504

Introduction. Heterostructures composed of superconductors and nonsuperconducting materials exhibit technologically relevant quantum phenomena [1–8]. Examples include superconducting qubits [9–11], microwave resonators [12], single-photon detectors [13], and AC Josephson junction lasers [14]. Superconducting heterostructures also form the basis for experimental methods such as point-contact spectroscopy [15–17] and scanning tunneling spectroscopy [18,19], enabling the determination of the superconducting gap and investigations of the phase diagram in unconventional superconductors [20–22].

The simplest superconducting heterostructure is a normal metal (N)–superconductor (S) junction. The low-bias transport is dominated by Andreev reflection (AR) [8,23,24]. In conventional AR, an incident electron is retroreflected as a hole of the opposite spin, and a Cooper pair is transmitted into the S layer. Since the Cooper pair carries a charge of $2e$ and zero heat, AR enhances electrical conductance and suppresses thermal conductance [25–27]. In a Josephson junction (S-N-S) [28], AR can occur repeatedly, resulting in Andreev bound states that carry a supercurrent across the junction. Josephson junctions enable technologies such as electrical and thermal interferometers [29,30].

The spin dependence of AR at superconducting interfaces causes the transport properties to change drastically when ferromagnetic (F) layers are introduced [31]. The exchange interaction splits the majority- and minority-spin bands in the F layer, which reduces the AR amplitude and consequently the conductance in a F-S junction [21,32]. However, finite spin-orbit coupling (SOC) at the interface enables tunable anisotropic spin-flipped AR, which can increase the electric and thermal conductance [33–36]. S-F-S Josephson junctions have been shown to exhibit spin-triplet pairing, potentially enabling superconducting spin currents and qubits [2,3,37–41]. However, the finite net magnetization of ferromagnets in superconducting spintronics presents a significant drawback for applications in nanoscale devices.

Antiferromagnets (AFs) are magnetically ordered materials with zero net magnetization and negligible stray fields, as well as intrinsic high-frequency dynamics. Thus, AFs are promising candidates for novel high-density and ultrafast spintronic-based nanodevices [42]. Based on these characteristics and recent experimental developments, the emerging field of antiferromagnetic spintronics has attracted intensive interest [43–52]. Additionally, the possible coexistence of antiferromagnetism with superconductivity [53–55] shows the great potential of antiferromagnetic materials for application in superconducting spintronics [31].

AF-S junctions have been theoretically shown to exhibit additional scattering processes that differ from those in N(F)-S junctions [56]. In Josephson junctions, these scattering processes create low-energy bound states [57] that lead to anomalous phase shifts [58] and atomic-scale 0-π transitions [59–62]. However, although the existence of Josephson supercurrents in S-AF-S junctions has been experimentally reported [63–68], other theoretical predictions have yet to be explored.

To our knowledge, the effect of these additional scattering processes on the electrical and thermal transport in AF-S bilayers remains an open question. In this Rapid Communication, we address this issue and point out unique experimental signatures in the electrical and thermal conductance.

Model. We consider a collinear, two-sublattice AF metal on a cubic lattice attached to a conventional s-wave superconductor. The AF and S are both semi-infinite and occupy the regions $z < 0$ and $z > 0$, respectively. We assume a compensated interface at $z = 0$.

To investigate the electrical and thermal transport, we use the Blonder-Tinkham-Klapwijk (BTK) scattering formalism

[25], where the conductances are determined by the reflection coefficients of the scattering matrix. We obtain the reflection coefficients by solving the Bogoliubov–de Gennes (BdG) equation.

The BdG Hamiltonian of an AF-S junction in the continuum limit consists of a Hamiltonian for itinerant charge carriers H_{e}, an antiferromagnetic exchange coupling H_{AF}, an interfacial barrier potential H_{I}, and a Hamiltonian modeling the S layer H_{S},

$$H = H_{\mathrm{e}} + H_{\mathrm{AF}} + H_{\mathrm{I}} + H_{\mathrm{S}}. \tag{1}$$

The Pauli matrices $\mathbf{s}$, $\boldsymbol{\sigma}$, and $\boldsymbol{\tau}$ denote the spin, sublattice, and charge degrees of freedom, respectively. We also define $\tau_4^{\pm} = \mathrm{diag}(1, \pm K)$, where K represents complex conjugation, and $\tau_{\pm} = (\tau_x \pm i\tau_y)/2$.

The Hamiltonian governing the motion of the itinerant charge carriers is [48,69,70]

$$H_{\mathrm{e}} = \gamma(\mathbf{p})\,\tau_z \otimes \sigma_x \otimes s_0 - \mu\,\tau_z \otimes \sigma_0 \otimes s_0, \tag{2}$$

where $\gamma(\mathbf{p}) = (\mathbf{p}^2 - \hbar^2 \boldsymbol{k}_0^2)/2m$ is the kinetic energy, $\mathbf{p} = -i\hbar\boldsymbol{\nabla}$ is the momentum operator, m is the effective mass of the charge carriers, $\boldsymbol{k}_0$ is the wave vector at which $\gamma(\hbar\mathbf{k}_0) = 0$, and $\hbar$ is the reduced Planck constant. The chemical potential is $\mu = \mu_{\mathrm{AF}}\Theta(-z) + \mu_{\mathrm{S}}\Theta(z)$, where $\Theta(\cdot)$ is the Heaviside step function.

The s-d exchange interaction between localized antiferromagnetic moments and itinerant spins reads [48,69,70]

$$H_{\mathrm{AF}} = J\,\tau_4^- \otimes \sigma_z \otimes (\mathbf{n}\cdot\boldsymbol{s}), \tag{3}$$

where $J = J_0\Theta(-z)$ denotes the interaction strength and $\mathbf{n} = (\sin\theta\cos\phi, \sin\theta\sin\phi, \cos\theta)$ is the uniform Néel vector. We assume strong anisotropy sets the direction of spins and suppresses quantum fluctuations. The interfacial potential is

$$H_{\mathrm{I}} = V\,\tau_z \otimes \sigma_0 \otimes s_0 + \lambda_{\mathrm{R}}\,\tau_4^+ \otimes \sigma_x \otimes [(\boldsymbol{s}\times\mathbf{q})\cdot\hat{z}], \tag{4}$$

where $V = V_0\delta(z)$ is the strength of the spin-independent potential barrier and $\lambda_{\mathrm{R}} = \lambda_0\delta(z)$ is the strength of the Rashba SOC (RSOC) [71] due to the inversion symmetry breaking in the z direction. These terms permit spin-conserving and spin-flipped reflection processes, respectively. AR and spin-flipped AR result in spin-singlet and spin-triplet Cooper pairs in S, respectively.

Finally, we model the S layer using a mean-field BCS Hamiltonian,

$$H_{\mathrm{S}} = \Delta(T)\,\tau_+ \otimes (\sigma_0 \otimes i s_y) + \mathrm{H.c.}, \tag{5}$$

where $\Delta(T) = \Delta_0 \tanh[1.74\sqrt{(T_c/T) - 1}]\Theta(z)$ is an interpolation formula for the temperature-dependent gap of an s-wave superconductor with a critical temperature T_c [72–74]. Δ_0 is the constant bulk value of the gap [57].

To determine the reflection coefficients, we solve the BdG eigenvalue problem,

$$H\psi = E\psi, \tag{6}$$

where ψ is an eigenvector with eigenvalue $E > 0$ (see the Supplemental Material [75]). The x and y directions are translationally invariant. Hence, the eigenvector takes the form $\psi = \chi e^{i\mathbf{q}_{\parallel}\cdot\mathbf{r}} e^{iq_z z}$, where $\mathbf{q}_{\parallel} = (q_x, q_y, 0)$ is the conserved component of the wave vector parallel to the interface and q_z is the wave-vector component normal to the interface. The spinor χ is expressed in the basis [75]

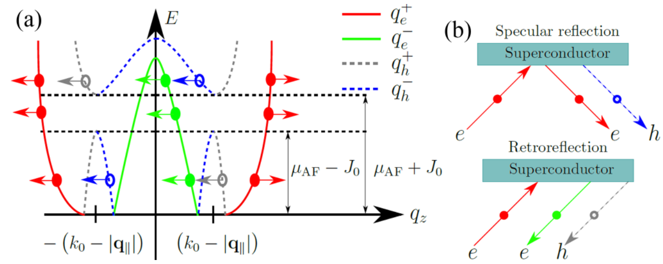

FIG. 1. (a) The allowed scattering processes [see Eq. (8)]. Electrons (holes) are drawn as solid (open) circles. Incoming (reflected) particles are represented by rightward (leftward) arrows. (b) A sketch of the possible scattering processes that can occur at an AF-S junction.

$$\chi = (A_{e\uparrow}, A_{e\downarrow}, B_{e\uparrow}, B_{e\downarrow}, A_{h\uparrow}, A_{h\downarrow}, B_{h\uparrow}, B_{h\downarrow}). \tag{7}$$

Here, A (B), $\uparrow$ ($\downarrow$), and e (h) refer to sublattice, spin, and charge degrees of freedom, respectively. Substituting the eigenvector into Eq. (6) for $z < 0$, gives the wave vectors $q_z = q_{e(h)}^{\pm}$ in the AF layer,

$$q_{e(h)}^{\pm} = \sqrt{k_0^2 - \mathbf{q}_{\parallel}^2 \pm \frac{2m}{\hbar^2}\sqrt{[E + (-)\mu_{\mathrm{AF}}]^2 - J^2}}. \tag{8}$$

Figure 1 shows a plot of the dispersion relations of the AF layer given in Eq. (8), where the possible scattering processes are identified. In contrast to an N(F)-S junction, an AF-S junction permits both specular AR and retro normal reflection (NR) [56–58].

In the following, we show how these two scattering mechanisms, i.e., retro NR and specular AR, affect the transport properties of AF-S junctions.

Thermoelectric coefficients. To study electrical and thermal transport, we assume that the AF is in contact with a biased reservoir, and that the S is in contact with a reference reservoir. Applying a bias voltage U or a temperature difference ΔT through the junction induces an electric current or a heat current, respectively. In the BTK formalism [25,26,76], the differential charge ($G_C = dI/dU$) and heat ($L_Q = dI/d\Delta T$) conductances read

$$G_C = \frac{Ae^2}{4\pi^3\hbar}\int dE\, d^2\mathbf{q}_{\parallel} \frac{1 - R_e + R_h}{4k_{\mathrm{B}}T\cosh^2\left(\frac{E - eU}{2k_{\mathrm{B}}T}\right)}, \tag{9a}$$

$$L_Q = \frac{Ak_{\mathrm{B}}}{4\pi^3\hbar}\int dE\, d^2\mathbf{q}_{\parallel} \frac{E^2(1 - R_e - R_h)}{[2k_{\mathrm{B}}(T + \Delta T)]^2\cosh^2\left[\frac{E}{2k_{\mathrm{B}}(T + \Delta T)}\right]}, \tag{9b}$$

where A and T are the interfacial area and the thermal equilibrium temperature, respectively. The total reflection probabilities for electrons (e) and holes (h) are

$$R_{e(h)} = \sum_s (R_{e(h),s}^+ + R_{e(h),s}^-). \tag{10}$$

Here, $R_{c,s}^{\pm}$ is the reflection probability for particles with wave vector $q_c^{\pm}$, where $c = e, h$ and $s = \uparrow, \downarrow$ [75]. AR results in a net charge transfer of $2e$, but zero heat transfer [77–79] across

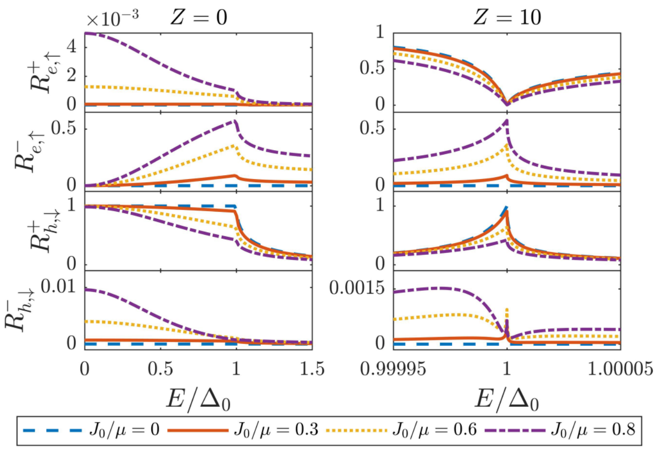

FIG. 2. The reflection probabilities as functions of the energy E/Δ_0, the barrier strength Z, and the exchange strength J_0/μ. The scattering processes associated with $R^-_{e,h}$ are absent at an N(F)-S junction; they are the result of the additional degrees of freedom in an AF. R^-_e and R^-_h correspond to retro NR and specular AR, respectively.

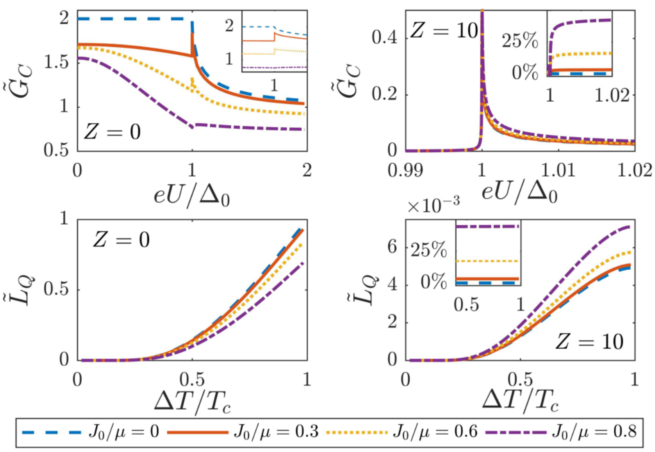

FIG. 3. The electrical conductance $\tilde{G}_C$ and the thermal conductance $\tilde{L}_Q$ as functions of the dimensionless voltage eU/Δ_0 and dimensionless temperature bias $\Delta T/T_c$, respectively, for different spin-independent barrier strengths Z and exchange strengths J_0/μ. The insets show the peak in the electrical conductance, and the percentage increase in the conductances as a function J_0/μ, respectively.

the interface; thus, AR increases the electrical conductance and decreases the thermal conductance.

Numerical parameters. Before presenting our numerical results, we introduce our dimensionless parameters: The spin-independent barrier strength $Z = V_0 m/\hbar^2 q_*$, the Rashba strength $\lambda = 2\lambda_0 m/\hbar^2 q_*$, and the exchange strength J_0/μ. Here, $q_*^2 = k_0^2 + q_F^2$, where $q_F^2 = 2m\mu/\hbar^2$. For simplicity, we set $\mu_{AF} = \mu_S = \mu$ and normalize the electrical and thermal conductance with respect to the corresponding Sharvin conductance [8]: $\tilde{G}_C = G_C/G_C^{Sh}$ and $\tilde{L}_Q = L_Q/L_Q^{Sh}$. The Sharvin electrical (thermal) conductance is the electrical (thermal) conductance evaluated in the limit $\Delta_0 = J_0 = Z = 0$, i.e., the response functions of a normal metal with perfect transmission: $G_C^{Sh} = e^2 q_*^2 A/4\pi^2\hbar$ and $L_Q^{Sh} = A k_B^2 T_c q_*^2/12\hbar$.

In our calculations, we estimate the effective mass to be $\hbar^2/2m = 0.5$ eV nm^2 based on a tight-binding model with typical material parameters [48,69,70]. Furthermore, the superconducting gap Δ_0 is several orders of magnitude smaller than the chemical potential μ. For concreteness, we set $\mu =$ 2 eV and allow the exchange strength to lie in the interval $0 < J_0/\mu < 1$, where the system is conducting. As $J_0/\mu \to 1$, the AF material becomes an insulator, and the transport properties vanish. We consider the temperature range $0 < T/T_c < 1$ so that superconductivity does not break down.

Calculation of reflection probabilities. Figure 2 shows the behavior of the reflection probabilities as functions of energy for different exchange strengths in both the transparent ($Z = 0$) and tunneling ($Z \gg 1$) regimes in the absence of RSOC.

For simplicity, we first consider a transparent interface ($Z = 0$) and the subgap regime ($E < \Delta_0$). In the normal metal limit ($J_0 = 0$), we find that retro AR is the dominant scattering process [25]. Retro NR and specular AR increase as the exchange interaction J_0 increases, because with the onset of J_0, the new scattering channels associated with the sublattice degrees of freedom become available. In the supergap regime ($E > \Delta_0$), electronlike and holelike charge carriers can propagate in the S layer.

If the interface is not transparent ($Z \neq 0$), AR is suppressed while NR is enhanced, because fewer electrons are allowed to enter the S layer to form Cooper pairs. Increasing J_0 leads to an increase in retro NR and a decrease in specular NR (see Fig. 2).

Electrical and thermal conductance. In the following, we elucidate experimental signatures in the response functions of the system. To simplify the discussion, we only consider the low-temperature limit $T \to 0$ in Eqs. (9a) and (9b) in the rest of this Rapid Communication. In Fig. 3, we plot the electrical conductance and the thermal conductance as functions of the voltage and temperature bias, respectively, for different exchange and barrier strengths in the absence of SOC.

First, we focus on the electrical conductance shown in Fig. 3. In the absence of a barrier and exchange interaction, the system behaves as a transparent N-S junction. In this case, each electron incident from the N layer enters the S layer and forms a Cooper pair, resulting in 100% retro AR; consequently, the electrical conductance is $\tilde{G}_C = 2$. As the exchange strength increases, retro NR eventually becomes the dominant scattering process. Thus, with increasing J_0, less total charge is transported across the junction and the electrical conductance decreases. In contrast to a F-S junction, we find a sharp finite peak in the electrical conductance at $eU/\Delta_0 = 1$.

In the tunneling limit ($Z = 10$), the electrical conductance is singular at $eU/\Delta_0 = 1$, which originates from the singularity in the density of states (DOS) in the S layer.

In contrast to the electrical conductance, the thermal conductance is suppressed by AR. The physical reason is that Cooper pairs carry finite charge but zero heat across the junction. Therefore, for the thermal conductance to be finite, the temperature must be so high that electronlike and holelike particles can be transmitted into the S layer. Since higher temperatures result in a greater transmission of particles, the thermal conductance increases with increasing temperature bias, as shown in Fig. 3.

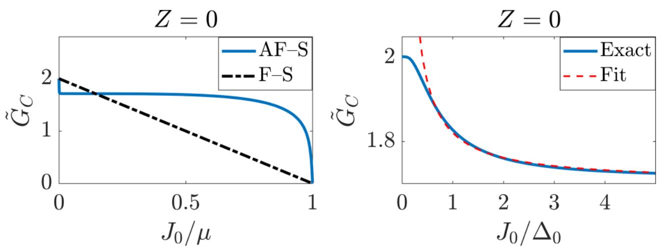

FIG. 4. Left: Zero-temperature electrical conductance $\tilde{G}_C$ of the system as a function of the exchange strength J_0/μ. The dashed-dotted line represents the electrical conductance of a F-S junction [32]. Right: The behavior of $\tilde{G}_C$ as a function J_0/Δ_0. The dashed red line represents a numerical fit of the electrical conductance, $\tilde{G}_C \sim (J/\Delta_0)^{-1.0}$.

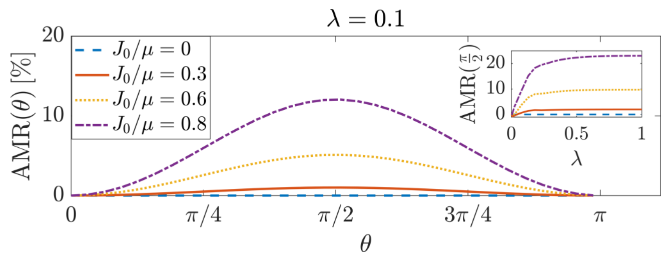

FIG. 5. The electrical AMR in an AF-S junction as a function of the orientation θ of the Néel vector and the exchange strength J_0/μ. The inset show the dependence of the AMR maxima on the RSOC strength λ.

In the transparent limit ($Z = 0$), the retro NR increases with increasing exchange strength. Since less particles are transmitted into the S layer, the thermal conductance decreases with increasing exchange strength. As the barrier strength increases, even fewer particles are transmitted into the S layer. In the tunneling limit ($Z = 10$), the thermal conductance is strongly suppressed.

Figure 3 shows that, in the transparent limit, the increase of exchange strength reduces both the electrical and thermal conductance; by contrast, in the tunneling regime, the increase in exchange strength increases both of them. This behavior occurs due to the interplay between the exchange interaction and the barrier in the supergap regime ($E > \Delta_0$), where tunneling into the S layer is also allowed. In the tunneling limit, the exchange interaction enhances the transmission of both electronlike and holelike particles into the S layer, consequently increasing the electrical and thermal conductance.

To compare the AF-S junction with the F-S junction, we plot the electrical conductance as a function of the exchange strength in Fig. 4. In the F-S junction, the electrical conductance decreases linearly with increasing exchange strength, $\tilde{G}_C \approx 2(1 - J_0/\mu)$ [32]. However, in the AF-S junction, the relationship between the electrical conductance and the exchange strength is more subtle. The electrical conductance decays rapidly at small J_0/μ, is almost constant for intermediate J_0/μ, and decays as $J_0/\mu \to 1$. We have checked that these features are robust by varying m, μ, and Δ_0 within the experimentally relevant intervals. The right panel of Fig. 4 shows that the electrical conductance decays rapidly with increasing exchange strength on an energy scale set by the superconducting gap. In the regime where $J_0 \ll \Delta_0$, the system behaves as an N-S junction, such that $\tilde{G}_C = 2$. In the regime $J_0 \sim \Delta_0$, we find that the reflection probabilities become dependent on the angle of incidence [75]. For electrons close to normal incidence, we find that retro AR dominates transport. For electrons with an angle of incidence nearly parallel to the interface, we find that retro AR is suppressed and specular NR is enhanced. This sudden enhancement of specular NR leads to the sharp decay of the electrical conductance observed in Fig. 4. Numerically, we find that $\tilde{G}_c \sim (J_0/\Delta_0)^{-1.0}$ [75].

In the regime $\Delta_0 \ll J_0 \ll \mu$, the DOS in the AF layer is approximately constant, and consequently, so is the electrical conductance [75]. As $J_0/\mu \to 1$, the AF layer starts to behave as an insulator, suppressing all transport properties.

Anisotropic magnetoresistance. So far, we have not considered the effect of finite interfacial RSOC, resulting from the inversion symmetry breaking at the interface. For finite interfacial RSOC, additional scattering channels are opened in which spin-flip scattering is allowed. Spin-flipped AR allows for the formation of spin-triplet Cooper pairs in the S layer [33,36,80]. Recently, it has been found that in F-S junctions, interfacial RSOC leads to a large anisotropic magnetoresistance (AMR) [33,81], while there is no AMR in N-S junctions.

In the AF layer, the spin quantization axis is determined by the Néel vector. Consequently, a finite interfacial RSOC leads to anisotropy in the electrical and thermal conductance for an AF-S junction. Since we consider only an interfacial RSOC with an inversion-breaking axis in the z direction, this AMR depends only on the Néel vector's polar angle θ.

Figure 5 shows electrical $\mathrm{AMR}(\theta) = 1 - \tilde{G}(0)/\tilde{G}(\theta)$ as a function of the Néel vector direction for a fixed RSOC strength. We find that the minima and maxima occur at $\theta = \{0, \pi\}$ and $\theta = \pi/2$, respectively. The inset shows that the maximum AMR increases with λ. The qualitative features of the electrical and thermal AMR is identical. Thus, similar to F-S junctions and in contrast to N-S junctions, AF-S junctions show a strong AMR. In an AF-N junction ($\Delta_0 \to 0$), the electrical (thermal) AMR is approximately 75% smaller (50% larger) than that in an AF-S junction. The simultaneous enhancement of the electrical AMR and diminution of the thermal AMR in an AF-S junction can be attributed to the finite AR in the presence of the S layer.

Concluding remarks. We demonstrate that the electrical and thermal conductance of AF-S junctions are qualitatively different from those of N(F)-S junctions due to the emergence of two scattering processes: Specular AR and retro NR. Furthermore, we show that there is a large AMR in the presence of a finite interfacial RSOC.

Our results reveal that superconducting spintronics based on antiferromagnetic materials, opens a fascinating playground for intriguing physical phenomena. We hope that this theoretical study will inspire further experimental work on AF-S heterostructures.

Acknowledgments. This research was supported by the European Research Council via Advanced Grant No. 669442, “Insulatronics,” the Research Council of Norway through its Centres of Excellence funding scheme, Project No. 262633, "QuSpin," and the Norwegian Financial Mechanism 2014-2021 Project No. 2019/34/H/ST3/00515, "2Dtronics." P.D. was supported by the Science and Engineering Board (SERB) of the Department of Science and Technology (DST) (File No. PDF/2016/001178) of India and by the Swedish Research Council (Vetenskapsrådet Grant No. 2018-03488) and the Knut and Alice Wallenberg Foundation through the Wallenberg Academy Fellows Program. P.D. acknowledges the warm hospitality of the QuSpin group during her visit when this work was initiated.

[1] R. Yan, G. Khalsa, S. Vishwanath, Y. Han, J. Wright, S. Rouvimov, D. S. Katzer, N. Nepal, B. P. Downey, D. A. Muller, H. G. Xing, D. J. Meyer, and D. Jena, Nature (London) **555**, 183 (2018).
[2] V. V. Ryazanov, V. A. Oboznov, A. Y. Rusanov, A. V. Veretennikov, A. A. Golubov, and J. Aarts, Phys. Rev. Lett. **86**, 2427 (2001).
[3] J. W. A. Robinson, J. D. S. Witt, and M. G. Blamire, Science **329**, 59 (2010).
[4] M. Eschrig, J. Kopu, J. C. Cuevas, and G. Schön, Phys. Rev. Lett. **90**, 137003 (2003).
[5] R. M. Lutchyn, J. D. Sau, and S. Das Sarma, Phys. Rev. Lett. **105**, 077001 (2010).
[6] B. Baek, W. H. Rippard, S. P. Benz, S. E. Russek, and P. D. Dresselhaus, Nat. Commun. **5**, 3888 (2014).
[7] M. Eschrig, Rep. Prog. Phys. **78**, 104501 (2015).
[8] I. Žutić, J. Fabian, and S. Das Sarma, Rev. Mod. Phys. **76**, 323 (2004).
[9] L. DiCarlo, J. M. Chow, J. M. Gambetta, L. S. Bishop, B. R. Johnson, D. I. Schuster, J. Majer, A. Blais, L. Frunzio, S. M. Girvin, and R. J. Schoelkopf, Nature (London) **460**, 240 (2009).
[10] J. E. Mooij, T. P. Orlando, L. Levitov, L. Tian, C. H. van der Wal, and S. Lloyd, Science **285**, 1036 (1999).
[11] F. Arute, K. Arya, R. Babbush, D. Bacon, J. C. Bardin, R. Barends, R. Biswas, S. Boixo, F. G. S. L. Brandao, D. A. Buell, B. Burkett, Y. Chen, Z. Chen, B. Chiaro, R. Collins, W. Courtney, A. Dunsworth, E. Farhi, B. Foxen, A. Fowler *et al.*, Nature (London) **574**, 505 (2019).
[12] M. J. Lancaster, T. S. M. Maclean, Z. Wu, A. Porch, P. Woodall, and N. N. Alford, IEE Proc., Part H: Microwaves, Antennas Propag. **139**, 149 (1992).
[13] G. N. Gol'tsman, O. Okunev, G. Chulkova, A. Lipatov, A. Semenov, K. Smirnov, B. Voronov, A. Dzardanov, C. Williams, and R. Sobolewski, Appl. Phys. Lett. **79**, 705 (2001).
[14] M. C. Cassidy, A. Bruno, S. Rubbert, M. Irfan, J. Kammhuber, R. N. Schouten, A. R. Akhmerov, and L. P. Kouwenhoven, Science **355**, 939 (2017).
[15] S. K. Upadhyay, A. Palanisami, R. N. Louie, and R. A. Buhrman, Phys. Rev. Lett. **81**, 3247 (1998).
[16] R. J. Soulen, J. M. Byers, M. S. Osofsky, B. Nadgorny, T. Ambrose, S. F. Cheng, P. R. Broussard, C. T. Tanaka, J. Nowak, J. S. Moodera, A. Barry, and J. M. D. Coey, Science **282**, 85 (1998).
[17] I. I. Mazin, Phys. Rev. Lett. **83**, 1427 (1999).
[18] R. Meservey and P. Tedrow, Phys. Rep. **238**, 173 (1994).
[19] M. Bode, Rep. Prog. Phys. **66**, 523 (2003).
[20] R. Gonnelli, D. Daghero, and M. Tortello, Curr. Opin. Solid State Mater. Sci. **17**, 72 (2013).
[21] G. Annunziata, M. Cuoco, P. Gentile, A. Romano, and C. Noce, Phys. Rev. B **83**, 094507 (2011).
[22] D. Daghero, M. Tortello, G. A. Ummarino, and R. S. Gonnelli, Rep. Prog. Phys. **74**, 124509 (2011).
[23] D. Daghero and R. S. Gonnelli, Supercond. Sci. Technol. **23**, 043001 (2010).
[24] W.-C. Lee and L. H. Greene, Rep. Prog. Phys. **79**, 094502 (2016).
[25] G. E. Blonder, M. Tinkham, and T. M. Klapwijk, Phys. Rev. B **25**, 4515 (1982).
[26] R. A. Riedel and P. F. Bagwell, Phys. Rev. B **48**, 15198 (1993).
[27] S. Lee, V. Stanev, X. Zhang, D. Stasak, J. Flowers, J. S. Higgins, S. Dai, T. Blum, X. Pan, V. M. Yakovenko, J. Paglione, R. L. Greene, V. Galitski, and I. Takeuchi, Nature (London) **570**, 344 (2019).
[28] B. Josephson, Phys. Lett. **1**, 251 (1962).
[29] F. Giazotto and M. J. Martínez-Pérez, Nature (London) **492**, 401 (2012).
[30] G. D. Guttman, B. Nathanson, E. Ben-Jacob, and D. J. Bergman, Phys. Rev. B **55**, 3849 (1997).
[31] J. Linder and J. W. A. Robinson, Nat. Phys. **11**, 307 (2015).
[32] M. J. M. de Jong and C. W. J. Beenakker, Phys. Rev. Lett. **74**, 1657 (1995).
[33] P. Högl, A. Matos-Abiague, I. Žutić, and J. Fabian, Phys. Rev. Lett. **115**, 116601 (2015).
[34] A. Costa, A. Matos-Abiague, and J. Fabian, Phys. Rev. B **100**, 060507(R) (2019).
[35] P. Dutta, A. Saha, and A. M. Jayannavar, Phys. Rev. B **96**, 115404 (2017).
[36] P. Dutta, K. R. Alves, and A. M. Black-Schaffer, Phys. Rev. B **102**, 094513 (2020).
[37] T. S. Khaire, M. A. Khasawneh, W. P. Pratt, and N. O. Birge, Phys. Rev. Lett. **104**, 137002 (2010).
[38] D. Sprungmann, K. Westerholt, H. Zabel, M. Weides, and H. Kohlstedt, Phys. Rev. B **82**, 060505(R) (2010).
[39] T. Yamashita, K. Tanikawa, S. Takahashi, and S. Maekawa, Phys. Rev. Lett. **95**, 097001 (2005).
[40] A. I. Buzdin, Rev. Mod. Phys. **77**, 935 (2005).
[41] A. I. Buzdin, L. N. Bulaevskii, and S. V. Panyukov, Pis'ma Zh. Eksp. Teor. Fiz. **35**, 147 (1982) [JETP Lett. **35**, 178 (1982)].
[42] V. Baltz, A. Manchon, M. Tsoi, T. Moriyama, T. Ono, and Y. Tserkovnyak, Rev. Mod. Phys. **90**, 015005 (2018).
[43] S. A. Siddiqui, J. Sklenar, K. Kang, M. J. Gilbert, A. Schleife, N. Mason, and A. Hoffmann, Metallic antiferromagnets, J. Appl. Phys. **128**, 040904 (2020).
[44] T. Jungwirth, X. Marti, P. Wadley, and J. Wunderlich, Nat. Nanotechnol. **11**, 231 (2016).
[45] B. G. Park, J. Wunderlich, X. Martí, V. Holý, Y. Kurosaki, M. Yamada, H. Yamamoto, A. Nishide, J. Hayakawa, H. Takahashi, A. B. Shick, and T. Jungwirth, Nat. Mater. **10**, 347 (2011).
[46] X. Martí, B. G. Park, J. Wunderlich, H. Reichlová, Y. Kurosaki, M. Yamada, H. Yamamoto, A. Nishide, J. Hayakawa, H.

Takahashi, and T. Jungwirth, Phys. Rev. Lett. **108**, 017201 (2012).
[47] H. Wang, C. Du, P. C. Hammel, and F. Yang, Phys. Rev. Lett. **113**, 097202 (2014).
[48] J. Železný, H. Gao, K. Výborný, J. Zemen, J. Mašek, A. Manchon, J. Wunderlich, J. Sinova, and T. Jungwirth, Phys. Rev. Lett. **113**, 157201 (2014).
[49] P. Wadley, B. Howells, J. Železný, C. Andrews, V. Hills, R. P. Campion, V. Novák, K. Olejník, F. Maccherozzi, S. S. Dhesi, S. Y. Martin, T. Wagner, J. Wunderlich, F. Freimuth, Y. Mokrousov, J. Kuneš, J. S. Chauhan, M. J. Grzybowski, A. W. Rushforth, K. W. Edmonds *et al.*, Science **351**, 587 (2016).
[50] R. Lebrun, A. Ross, S. A. Bender, A. Qaiumzadeh, L. Baldrati, J. Cramer, A. Brataas, R. A. Duine, and M. Kläui, Nature (London) **561**, 222 (2018).
[51] J. Li, C. B. Wilson, R. Cheng, M. Lohmann, M. Kavand, W. Yuan, M. Aldosary, N. Agladze, P. Wei, M. S. Sherwin, and J. Shi, Nature (London) **578**, 70 (2020).
[52] P. Vaidya, S. A. Morley, J. van Tol, Y. Liu, R. Cheng, A. Brataas, D. Lederman, and E. del Barco, Science **368**, 160 (2020).
[53] M. Feldbacher, F. F. Assaad, F. Hébert, and G. G. Batrouni, Phys. Rev. Lett. **91**, 056401 (2003).
[54] E. Demler, W. Hanke, and S.-C. Zhang, Rev. Mod. Phys. **76**, 909 (2004).
[55] J. Kaczmarczyk and J. Spałek, Phys. Rev. B **84**, 125140 (2011).
[56] I. V. Bobkova, P. J. Hirschfeld, and Y. S. Barash, Phys. Rev. Lett. **94**, 037005 (2005).
[57] B. M. Andersen, I. V. Bobkova, P. J. Hirschfeld, and Y. S. Barash, Phys. Rev. B **72**, 184510 (2005).
[58] D. S. Rabinovich, I. V. Bobkova, and A. M. Bobkov, Phys. Rev. Research **1**, 033095 (2019).
[59] B. M. Andersen, I. V. Bobkova, P. J. Hirschfeld, and Y. S. Barash, Phys. Rev. Lett. **96**, 117005 (2006).
[60] X. Zhou, M. Lan, Y. Ye, Y. Feng, X. Zhai, L. Gong, H. Wang, J. Zhao, and Y. Xu, Europhys. Lett. **125**, 37001 (2019).
[61] L. Bulaevskii, R. Eneias, and A. Ferraz, Phys. Rev. B **95**, 104513 (2017).
[62] H. Enoksen, J. Linder, and A. Sudbø, Phys. Rev. B **88**, 214512 (2013).
[63] C. Bell, E. J. Tarte, G. Burnell, C. W. Leung, D.-J. Kang, and M. G. Blamire, Phys. Rev. B **68**, 144517 (2003).
[64] P. Komissinskiy, G. A. Ovsyannikov, I. V. Borisenko, Y. V. Kislinskii, K. Y. Constantinian, A. V. Zaitsev, and D. Winkler, Phys. Rev. Lett. **99**, 017004 (2007).
[65] M. H. Bener, D. Tikhonov, I. A. Garifullin, K. Westerholt, and H. Zabel, J. Phys: Condens. Matter **14**, 8687 (2002).
[66] K. Y. Constantinian, Y. V. Kislinskii, G. A. Ovsyannikov, A. V. Shadrin, A. E. Sheyerman, A. L. Vasil'ev, M. Y. Presnyakov, and P. V. Komissinskiy, Phys. Solid State **55**, 461 (2013).
[67] B. L. Wu, Y. M. Yang, Z. B. Guo, Y. H. Wu, and J. J. Qiu, Appl. Phys. Lett. **103**, 152602 (2013).
[68] J. J. Hauser, H. C. Theuerer, and N. R. Werthamer, Phys. Rev. **142**, 118 (1966).
[69] A. Qaiumzadeh, I. A. Ado, R. A. Duine, M. Titov, and A. Brataas, Phys. Rev. Lett. **120**, 197202 (2018).
[70] J. Železný, H. Gao, A. Manchon, F. Freimuth, Y. Mokrousov, J. Zemen, J. Mašek, J. Sinova, and T. Jungwirth, Phys. Rev. B **95**, 014403 (2017).
[71] Y. A. Bychkov and E. I. Rashba, J. Phys. C: Solid State Phys. **17**, 6039 (1984).
[72] K. Senapati, M. G. Blamire, and Z. H. Barber, Nat. Mater. **10**, 849 (2011).
[73] D. Guterding, S. Diehl, M. Altmeyer, T. Methfessel, U. Tutsch, H. Schubert, M. Lang, J. Müller, M. Huth, H. O. Jeschke, R. Valentí, M. Jourdan, and H.-J. Elmers, Phys. Rev. Lett. **116**, 237001 (2016).
[74] In this Rapid Communication, we have neglected the dependence of T_c on the direction of the order parameter, typically originating from the strong SOC present in, e.g., F–heavy metal–S structures and the proximity effects [82]. We expect that T_c can depend on the orientation of **n** in AF–heavy metal–S trilayers.
[75] See Supplemental Material at http://link.aps.org/supplemental/10.1103/PhysRevB.102.140504 for additional details on wave functions in the AF, calculation of reflection amplitudes, normal metal limit, electrical conductance, and DOS in the AF.
[76] S. Chaudhuri and P. F. Bagwell, Phys. Rev. B **51**, 16936 (1995).
[77] E. V. Bezuglyi and V. Vinokur, Phys. Rev. Lett. **91**, 137002 (2003).
[78] J. A. Sauls, Philos. Trans. R. Soc., A **376**, 20180140 (2018).
[79] T. Yokoyama, J. Linder, and A. Sudbø, Phys. Rev. B **77**, 132503 (2008).
[80] T. Vezin, C. Shen, J. E. Han, and I. Žutić, Phys. Rev. B **101**, 014515 (2020).
[81] I. Martínez, P. Högl, C. González-Ruano, J. P. Cascales, C. Tiusan, Y. Lu, M. Hehn, A. Matos-Abiague, J. Fabian, I. Žutić, and F. G. Aliev, Phys. Rev. Applied **13**, 014030 (2020).
[82] C. González-Ruano, L. G. Johnsen, D. Caso, C. Tiusan, M. Hehn, N. Banerjee, J. Linder, and F. G. Aliev, Phys. Rev. B **102**, 020405(R) (2020).